FORTE 2.0: a fast, parallel and flexible coupled climate model

Adam T. Blaker[1], Manoj Joshi[2], Bablu Sinha[1], David P. Stevens[3], Robin S. Smith[4], and Joël J.-M. Hirschi[1]

[1]National Oceanography Centre, European Way, Southampton, SO14 3ZH, UK
[2]Climatic Research Unit, School of Environmental Sciences, University of East Anglia, Norwich, UK
[3]Centre for Ocean and Atmospheric Sciences, School of Mathematics, University of East Anglia, Norwich, UK
[4]NCAS, Dept. of Meteorology, University of Reading, Reading, UK

Correspondence to: A. T. Blaker (atb299@noc.ac.uk)

Abstract.

FORTE 2.0 is an intermediate resolution coupled Ocean Atmosphere General Circulation Model (AOGCM) consisting of IGCM4, a T42 spectral atmosphere with 35 σ layers, coupled to MOMA, a 2° × 2° ocean with 15 z layer depth levels. It is capable of producing a stable climate for long integrations without the need for flux adjustments. One flexibility afforded by the IGCM4 atmosphere is the ability to configure the atmosphere with either 35 σ layers (troposphere and stratosphere) or 20 σ layers (troposphere only). This enables experimental designs for exploring the roles of the troposphere and stratosphere, and the faster integration of the 20 σ layer configuration enables longer duration studies on modest hardware. A description of FORTE 2.0 is given, followed by analysis of a 2000 year long control integration.

1 Introduction

Numerical models of the coupled (ocean-atmosphere) climate system are important tools for studying the Earth's climate. They provide insight into phenomena which are difficult to observe directly, such as the Atlantic Meridional Overturning Circulation (AMOC) or the effects of increasing atmospheric CO_2. They can also be used to test hypotheses about the global climate and the world we live in. In a climate model it is possible to study the climate response to extreme events such as loss of ice cover (and the resulting change in albedo). Whilst the results in terms of quantitative changes to temperature, precipitation, and other climate variables should be treated with caution, it is possible to examine the processes which lead to the predicted changes.

There is a broad spectrum of coupled climate models. At one end of the spectrum are coarse resolution simplified models designed to run millennial scale experiments quickly and for minimal computational cost, both in terms of computing power and memory resources (e. g. GENIE (Marsh et al., 2007), CLIMBER (Montoya et al., 2005), UVic (Weaver, 2004)). At the opposite end of the spectrum, high resolution (<0.1°- 0.5° ocean) models (e.g. those contributing to the CMIP6 HighResMIP (Haarsma et al., 2016) such as HadGEM3-GC3.1 (Roberts et al., 2019), and HiGEM (Shaffrey et al., 2009)). Between the two extremes are the intermediate resolution models (e.g. ECBilt (Haarsma et al., 1996), HadCM3 (Gordon et al., 2000), FAMOUS (Smith et al., 2008)), including most of the coupled climate models contributing to CMIP3 (Meehl et al., 2007), CMIP5 (Taylor et al., 2012) and CMIP6 (Eyring et al., 2016). It is worth noting that model development does not equate solely to increase in

horizontal resolution. Inclusion of more, or better parameterised, Earth System processes can be equally if not more important developments (e.g. Sellar et al., 2019).

Sinha and Smith (2002) developed FORTE (Fast Ocean Rapid Troposphere Experiment), a fast and flexible coupled climate model, for the purposes of climate studies. FORTE's speed and flexibility meant that the original model was an ideal educational

5 and research tool. A variety of experiments that used FORTE to study ocean and/or climate phenomena have been published (Buchan et al., 2014; Hunt et al., 2013; Sinha et al., 2012; Wilson et al., 2009; Atkinson et al., 2009; Grist et al., 2008; Blaker et al., 2006) although there is no comprehensive, peer-reviewed publication describing the model itself. Although most studies used FORTE with a T42 resolution atmosphere and 2°ocean, a version of FORTE using a T21 resolution atmosphere and 4°ocean has also been used for idealised experiments (e.g. Smith et al., 2004, 2006).

10 A new version of the atmosphere component of FORTE was released in 2015, and a desire to perform coupled experiments once again resulted in a refresh of FORTE. To avoid confusion with earlier endeavours, but at the same time make clear the ancestry of the model we decided to refer to the refreshed model as FORTE 2.0. This paper describes the coupled model and its components and demonstrates that FORTE 2.0 produces a realistic and stable climate without the need for flux adjustments. The control integration described is a 2000 year long integration starting from rest with the Levitus (temperature, salinity)

15 climatology (Levitus and Boyer, 1998; Levitus et al., 1998) and pre-industrial atmospheric concentrations of CO_2. The model is forced solely by incoming solar radiation at the top of the atmosphere. The rest of this paper is organised as follows: Section 2 gives a description of FORTE 2.0; Section 3 presents the model spin-up; Section 4 presents the control climate; Section 5 discusses the main modes of climate variability in the model; Section 6 concludes.

2   Model Description

20 FORTE 2.0 is a global coupled ocean-atmosphere general circulation model consisting of a 2° resolution configuration of the MOMA (Modular Ocean Model - Array) (Webb, 1996) ocean model coupled to a T42 (approximately 2.8°) configuration of the IGCM4 (Intermediate General Circulation Model 4) (Joshi et al., 2015) atmosphere model. FORTE 2.0 is an updated incarnation of FORTE (Fast Ocean Rapid Troposphere Experiment) (Sinha and Smith, 2002; Smith et al., 2004), with the most significant change being an update of the atmosphere from IGCM3 (Forster et al., 2000) to IGCM4 (Joshi et al., 2015).

25 The ocean and atmosphere components of FORTE 2.0 are coupled once per model day using OASIS version 2.3 (Terray et al., 1999) and PVM version 3.4.6 (Parallel Virtual Machine, see http://www.csm.ornl.gov/pvm/, Geist et al. (1994)). Integration is relatively fast (~100 model years per wallclock day on a 28 core 2.4GHz Intel Broadwell CPU) and the model can be run on a desktop computer, making it ideal for experiments where more complex higher resolution models are resource limited. The retention of the full primitive equations for fluid flow in both atmosphere and ocean allows more realistic simulations than

30 possible with Earth Models of Intermediate Complexity (EMICs). In addition, FORTE 2.0 is readily configurable, allowing experiments with idealized configurations of coastlines, orography, and ocean bottom topography.

2.1 The atmosphere component

The atmosphere component of FORTE 2.0 is IGCM4 (Joshi et al., 2015), run with a T42 spectral resolution. A longitudinally regular grid is used for advection and diabatic processes, with a grid spacing of 2.8°, and a Gaussian grid in latitude, with an irregular grid spacing of approximately 2.8°. The resolution is sufficient to enable stable climate integrations without the need

5 for flux adjustments. There are two pre-configured choices for the number of vertical levels: a troposphere only atmosphere represented by 20 σ levels (L20) which extends to around 25 km altitude, or a 35 σ level configuration (L35) which includes the stratosphere and extends to around 65 km altitude. The model is run with 96 (L35) or 72 (L20) time steps per day. Orography is derived from the US Naval 1/6th degree resolution dataset. IGCM4 is MPI parallelised, and at this resolution integration on 16-32 cores achieves the best performance.

10 Atmospheric convection is dealt with via a Betts-Miller scheme (Betts and Miller, 1993). Low, medium and high layer cloud and convective clouds amount are represented, based on a critical relative humidity criterion (see the Appendix of Forster et al. (2000)). The formula which determines low-level cloud amount has an additional factor of 50% compared to that used by Forster et al. (2000) to correct a cold bias within the tropical ocean which led to unrealistic circulation in the Pacific. In addition to variation with solar zenith angle (and hence latitude), sea surface albedo is increased away from polar regions to

15 compensate for the absence of aerosols which would otherwise scatter incoming solar radiation. Land grid boxes are assigned a vegetation index, one of 24 pre-defined vegetation types, which determine the albedo and roughness length.

Coupling to the dynamic ocean model requires some changes to the surface boundary layer. In order to conserve water it is necessary to account for soil moisture and implement river runoff. Soil moisture for each land grid box is represented as a bucket, or reservoir, 0.5 m in depth. Excess water, i.e. when the volume of water is greater than the volume of the bucket,

20 is accumulated and added to the ocean as runoff at each coupling timestep. The land surface is divided into catchment basins and the accumulated runoff is distributed between a list of ocean cells that represent river mouths. Runoff accumulated over Antarctica is distributed uniformly over the ocean south of 55°S, as a simplistic representation of iceberg calving and melting. Additionally, land snow cover is capped at a maximum thickness of 4 m. Excess snow over Antarctica and the Arctic region is treated separately as an additional runoff term that represents iceberg melting and calving. As with the soil moisture, runoff

25 from excess snow over Antarctica is distributed uniformly over the ocean south of 55°S. Excess snow melt over the Arctic is handled similarly, with a uniform distribution over the ocean north of 66°N.

To improve the representation of the effects of surface roughness on momentum exchange a wind-dependent drag coefficient, C_d, is implemented, such that $C_d = C_d^0 + 5.6e^{-5} * \text{windspeed}$ (Wu, 1980). This gives a maximum $C_d = 0.003$ at windspeed of 40 m s^{-1} without ice cover. C_d^0 is the drag coefficient over ocean cells, calculated using a globally uniform value for surface

30 roughness over open ocean.

At present FORTE 2.0 does not include dynamic sea-ice representation. Instead, sea ice is represented by a barrier to heat fluxes between the ocean and atmosphere component, which is imposed when the sea surface temperature reaches 271 K, and surface albedo is increased to 0.6 to represent ice cover. The albedo continues to linearly increase, reaching 0.8 at 261 K as a means to represent the albedo effects of snow on ice. Once the albedo reaches 0.8 it will not reduce until the ice has melted.

Parameter	Value ($m^2\ s^{-1}$)
Horizontal viscosity	4.0×10^3
Isopycnal tracer diffusivity	3.0×10^3
Isopycnal thickness diffusivity	2.0×10^3
Steep slope horizontal diffusivity	2.0×10^3
Vertical diffusion coefficient	5.0×10^{-5}
Vertical viscosity coefficient	1.0×10^{-3}
Bottom drag coefficient	0.001
Max. slope of isopycnals	0.002

Table 1. Mixing parameters in MOMA.

There is no advection of sea ice, and salinity and runoff fluxes remain unaffected. Sea-surface temperature (SST) under ice is relaxed toward the freezing point of seawater (-1.8° C) on a 10-day timescale.

2.2 The ocean component

The ocean component of FORTE 2.0 is MOMA (Modular Ocean Model - Array, Webb (1996)), a version of the GFDL
MOM (Modular Ocean Model) (Pacanowski et al., 1990) coded to work more efficiently on array processors, which solves the primitive equations discretized using finite differences on an Arakawa B grid (Arakawa, 1966). It has a linear free surface (Killworth et al., 1991) and uses 'full cell' ocean bathymetry. In the configuration used for this integration the ocean horizontal resolution is 2° x 2°, with 15 z-layer levels, increasing in thickness with depth from 30 m at the surface to 800 m at the bottom. A polar island, comprising the top row of grid cells, is required in the Arctic to prevent numerical instability due to convergence of lines of longitude. There are 64 baroclinic time steps per day (22.5 minute time steps) implemented using the modified split QUICK (MSQ) advection scheme (Webb et al., 1998). MOMA is parallelised using OpenMP and running on 4-6 cores is typically sufficient to match the IGCM4 performance.

Bathymetry is derived from the ETOPO5 (1988) 1/12° resolution dataset, and interpolated onto the model resolution. Due to the horizontal resolution, in order to encourage dense water formation and flow between the Nordic Seas and North Atlantic, bathymetry is manually excavated in a manner simialr to HadCM3 (Gordon et al., 2000). The Bering, Gibraltar and Kattegat/Skagerrak Straits are represented by a single grid box which, due to the Arakawa B grid, means that there is no advection through them, but diffusion of potential temperature (T) and salinity (S) does occur.

Ocean isopycnal mixing is represented in MOMA through the isoneutral mixing scheme of Griffies et al. (1998). The eddy-stirring process of Gent and McWilliams (1990) is introduced as a skew flux (Griffies, 1998). Where isopycnal slopes become large, exponential tapering scales isoneutral diffusivities to zero as the slope increases (Danabasoglu and McWilliams, 1995). The isopycnal mixing parameters used for the control simulation described in section 3 are shown in Table 1.

To ameliorate some of the shortcomings identified in earlier FORTE simulations some additional changes have been made to MOMA. Firstly, the background vertical diffusion, κ, is set to be stability dependent (Gargett, 1984), albeit with the surface to sea floor potential temperature gradient as a simple proxy for stability, such that

$$\kappa_s = (0.3 + 1.7\mathrm{e}^{-(0.15[\max(T_s, T_b) - T_b])^2}) \times 10^{-4}\,\mathrm{m^2 s^{-1}},$$

$$\kappa = \kappa_s + (2 \times 10^{-4} - \kappa_s)z/H\,\mathrm{m^2 s^{-1}},$$

where T_s is the surface potential temperature, T_b is the bottom potential temperature, z is depth and H is the local total depth of the ocean. Thus the vertical diffusivity takes a maximum value of $2 \times 10^{-4}\,\mathrm{m^2 s^{-1}}$ at the sea floor and at high latitudes, with lower values, approaching $3 \times 10^{-5}\,\mathrm{m^2 s^{-1}}$ in the upper ocean at low latitudes.

Secondly, starting from 5° N/S the horizontal diffusion in the surface layer increases towards the Equator from its default value to 20 times this value at the Equator, to counteract equatorial upwelling and, in a simple way, parameterise the eddy heat convergence associated with tropical instability waves which was highlighted by Shaffrey et al. (2009).

3 Spinup of the control integration

The control integration of FORTE 2.0 starts from rest using the 35 σ layer atmosphere configuration and with initial ocean temperature and salinity fields from Levitus and Boyer (1998) and Levitus et al. (1998) interpolated onto the ocean model grid. The surface heat flux into the ocean is initially positive (up to 1.5 W m^{-2}) but the imbalance reduces to less than 0.5 W m^{-2} after a few decades and then stabilises and remains within 0.1-0.2 W m^{-2} throughout the remainder of the integration (Fig. 1 a)). The time average water budget closes to within -0.2 mm/year, after an initial adjustment in the first year of the integration (Fig. 1 b)). The global average sea surface temperature (SST) settles within 100 years to a value around 19.1°C , whilst sea surface salinity (SSS) adjusts more slowly, maintaining a value of around 35.15 PSU after 1000 years of integration (Figs. 1 c) and d)). The mean SST is 0.9°C warmer than the initial state provided by Levitus 1998 (18.2°C). The volume average ocean potential temperature warms by 0.3°C over the first 500 years, and then cools more steadily, at a rate of approximately 0.005°C/century. Salinity shows a gradual trend of 0.000125 PSU/century after an initial adjustment), which is a reflection of the small imbalance in the fresh water fluxes.

Global averaged time series of temperature and salinity as functions of latitude and depth are presented in Fig. 2. The time-latitude plots show an initial strong warming of the Southern Ocean that is not density compensated by an increase in salinity at the same latitudes. The onset of this warming occurs quickly and then remains stable for the remainder of the 2000-year integration. A minimal bias develops in the tropical and equatorial regions. In the northern hemisphere higher latitudes there is a strong cooling, that (partly) coincides with a freshening. Analysis of the spatial SST and SSS biases presented later in this paper shows that these anomalies are located in the Nordic Seas. This pattern develops over the first 500 years of the simulation, and then remains stable for the rest of the integration. The SST bias is within the range of that found in the CMIP5 ensemble (Flato et al., 2013).
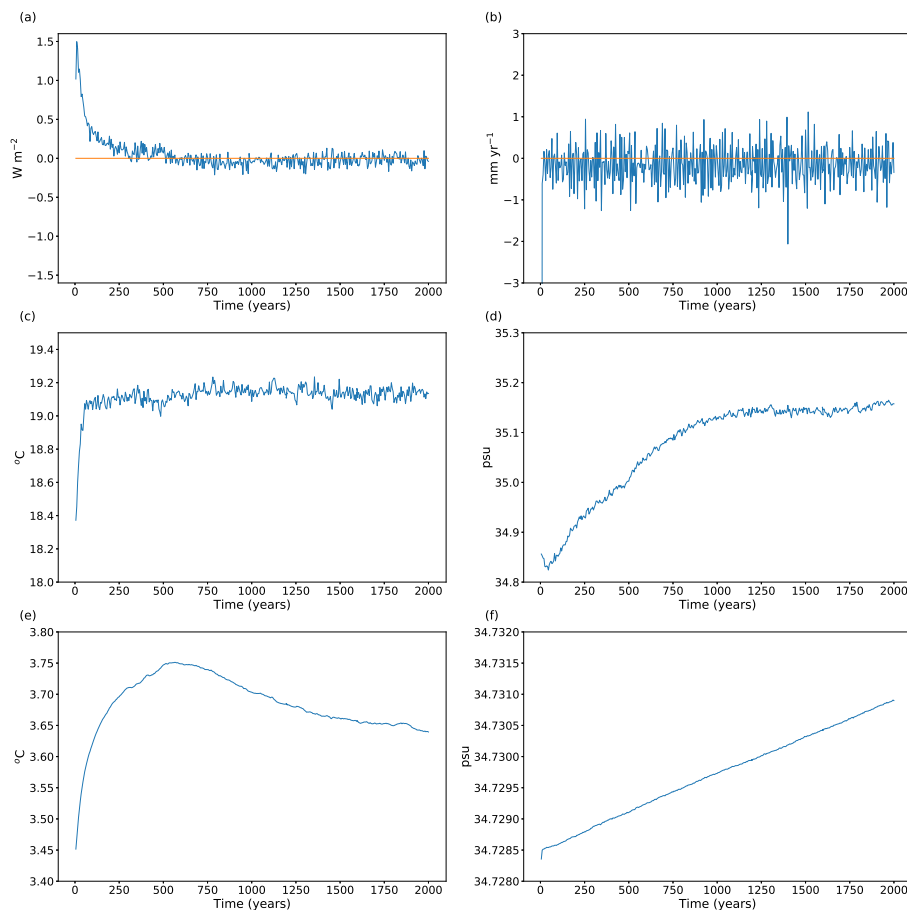
Figure 1. Time series of global mean a) surface heat flux (W m^{-2}) and b) surface water flux (mm/year) into the ocean, c) SST (°C) and d) SSS, and volume averaged e) potential temperature and f) salinity.

The time-depth series of potential temperature (Fig. 2 c) compares reasonably with those of other, higher resolution, models such as HadCM3, HadGEM1 and CHIME (Fig. 7 in Johns et al. (2006), Fig. 3 in Megann et al. (2010)). FORTE 2.0 warms above 1500 m, with the maximum difference from observed values reaching +1.6°C between 400 and 500 m depth. At depths below 4000 m the ocean cools initially, with differences from observations at 5000 m reaching -0.2°C. Differences in salinity

5 from observations, again shown as a global averaged time-depth series, are small (Fig. 2 d). Differences of +0.3 PSU occur between 300 m and 600 m, whilst below 1500 m they are negative and reach a maximum of -0.15 PSU in the abyssal ocean.

The time series of the maximum AMOC at 30°N is presented in Fig. 3. During the first 300 years of integration a relatively stable 16-18 Sv is maintained, after which there is a reduction of around 3 Sv to 13-15 Sv. These values are maintained for the remainder of the 2000 year integration. These values are within the range of those from the CMIP5 ensemble (Heuzé et al.,

10 2015). The standard deviation of the AMOC based on monthly mean values is 3.5 Sv, which is in reasonable agreement with
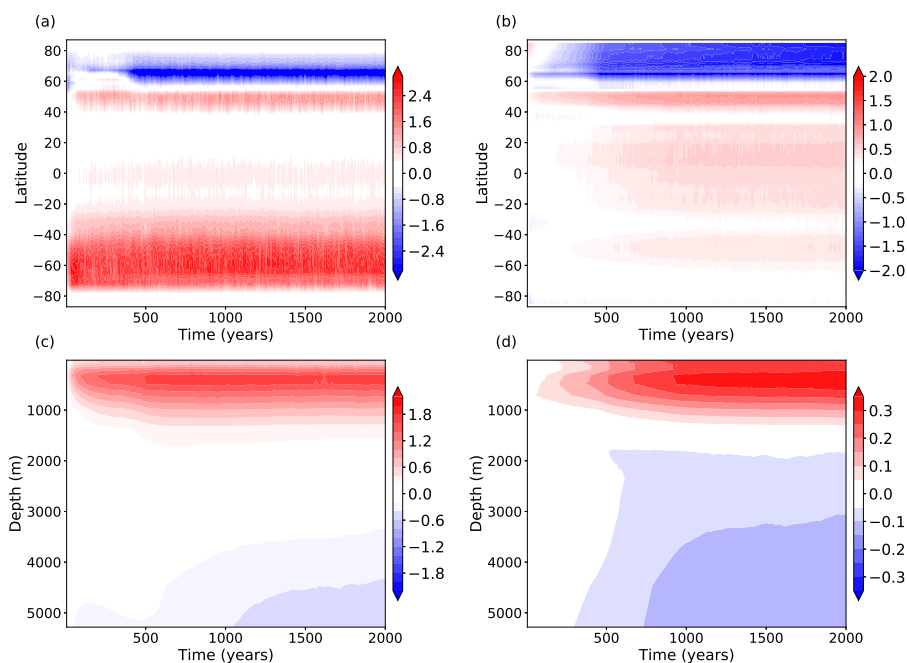
Figure 2. Time-latitude plots of drift in annual mean sea surface (a) temperature (°C), and (b) salinity (PSU) and time-depth series of global drift in annual mean (c) potential temperature (°C) and (d) salinity (PSU). Drift is relative to initial conditions.
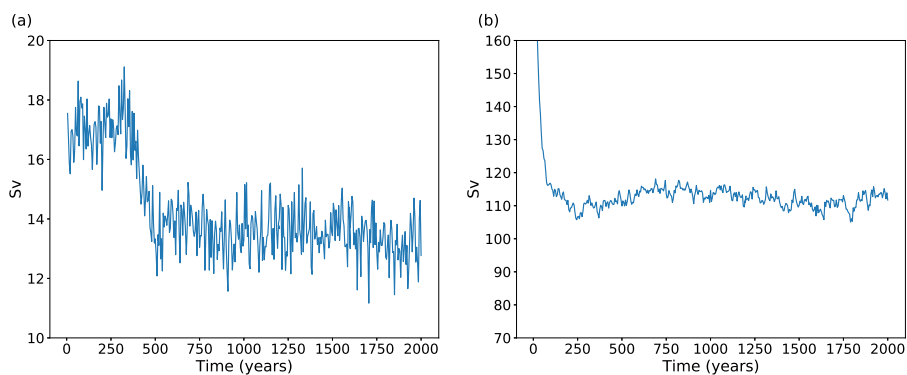
Figure 3. Time series of a) the 5-year mean Atlantic MOC, and b) Drake Passage transport in the control integration

the magnitude of observed variability (McCarthy et al., 2012). Other than the adjustment in the first 500 years, there is little evidence of emergent decadal or multidecadal variability over the course of the control integration, the peak-to-peak range over the last 1500 years of the integration being 3-4 Sv.

Transport through Drake Passage weakens rapidly from an initial value of > 160 Sv and from year 200 it settles around
5 110-115 Sv. This is lower than the recent observation-based estimate of 173 Sv (Donohue et al., 2016) or previous estimates values of around 130-140 Sv (e.g. Cunningham et al., 2003), but within the range seen in other coupled climate models (Russell et al., 2006).

4   The control climate

After the 2000 year spinup, the frequency of output was increased to monthly and a 25 year long integration was performed.
10 In this section the control climate during this 25 year period is presented.

4.1   The Atmosphere

Annual time mean surface air temperatures (SATs) in the tropics are 25°C, with some regions over land reaching 30-35°C. The Arctic reaches -20°C, with temperatures over Greenland reaching as low as -40°C and the interior of Antarctica reaches as low as -60°C (Fig. 4 a)).
15 Contours of annual average mean sea level pressure anomalies, displayed in Fig. 5 a), show the expected bands of high pressure over the subtropical oceans (e.g. the Azores and North Pacific Highs) and over the polar regions and low pressure cells at mid latitudes (e.g. Icelandic and Aleutian Lows) and over the Equatorial regions.

Seasonal SAT variability over the tropical ocean is low, whilst variations in SAT over land can be 15-20°C (Fig. 4 b), c) and d)). Arctic and Antarctic seasonal SAT variability is 40-45°C, with the coldest regions of Antarctica reaching as low as
20 -85°C during July. Contours of sea level pressure show the intensification of the surface winds over the midlatitudes in both southern and northern hemispheres during the winter season. We note that the Siberian high is not very intense for mean January conditions and this appears to have the effect of allowing the Icelandic Low to expand and displace eastwards over Scandinavia, resulting in a displacement of the winter NAO pattern compared with observations (see section 5).

The pattern of annual mean precipitation (Fig. 4 e)) shows reasonable agreement with observations (Adler et al., 2003),
25 namely the regions of high precipitation over the regions of the northern hemisphere oceanic western boundary currents (up to 6 mm/day and extending to northwestern Canada and north west Europe as in the observations), as well as high values (10-12 mm/day) over tropical Africa and South America, Indonesia and over the Inter Tropical Convergence Zones in the Atlantic and Pacific Oceans. Very low values (0-1 mm/day) are seen over the polar regions, the subtropical desert regions (terrestrial and oceanic) and (unrealistically) over the equatorial Pacific. A major difference with the observed distribution is the South
30 Pacific ITCZ, which is narrow and predominantly zonal in the model solution, whereas based on observations we would expect a broader north-west to south-east oriented region. Figures 4 f), g) and h) show that the seasonal maxima in the ITCZ regions
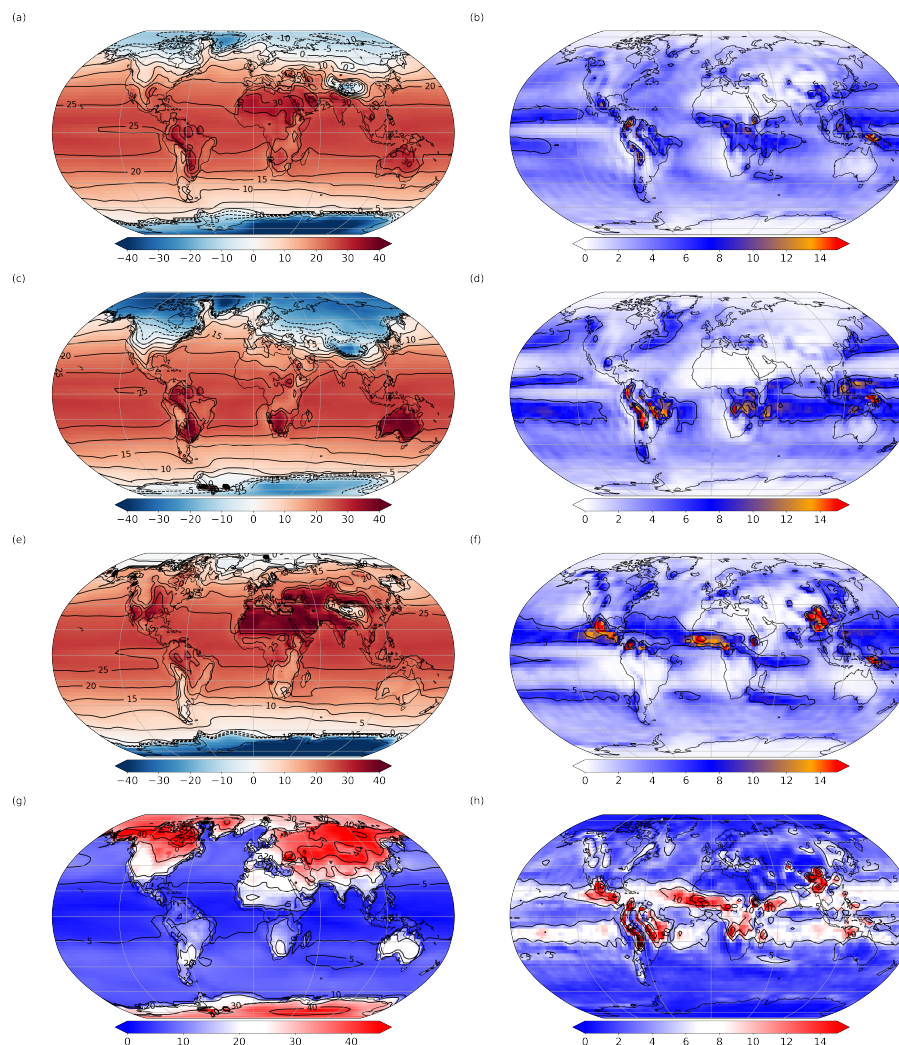
Figure 4. Time mean (years 2001-2025) plots of: surface air temperature (°C) for a) annual mean, c) January, e) July, g) seasonal range; and precipitation (mm/day) for b) annual mean, d) January, f) July, and h) seasonal range.

are frequently in excess of 15 mm/day. Conversely, the model predicts too little precipitation in the summer months in both hemispheres.

Time mean zonal wind for both summer and winter is shown in Fig. 6 as a function of latitude and pressure. The model exhibits northern and southern hemisphere jet streams at around 40°S and 40°N at 200 hPa. The southern jet stream exhibits a lower seasonal range (28–36 m s^{-1}) than the northern jet stream (12–36 m s^{-1}). Surface westerlies and easterlies are of order ±0–4 m s^{-1} in the annual mean.
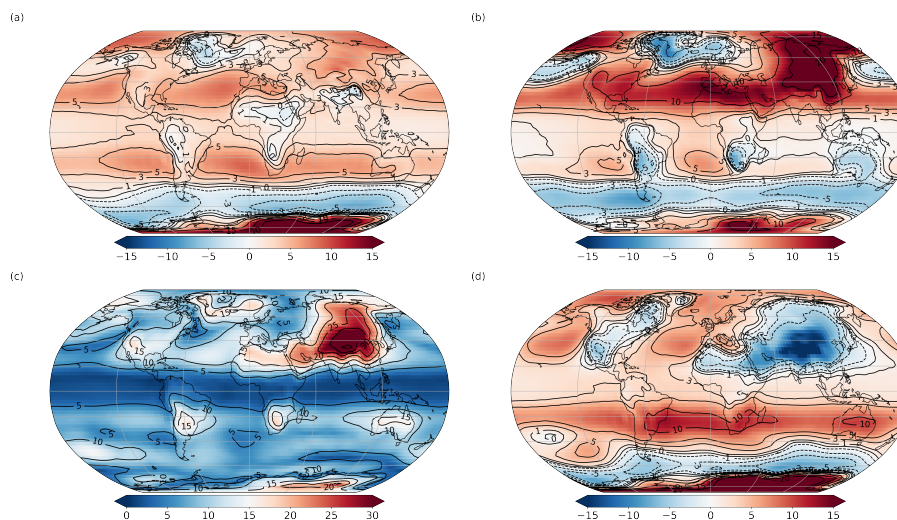
Figure 5. Time mean (years 2001-2025) plots of: sea level pressure anomaly (mb) for a) annual mean, b) January, c) seasonal range, d) July.
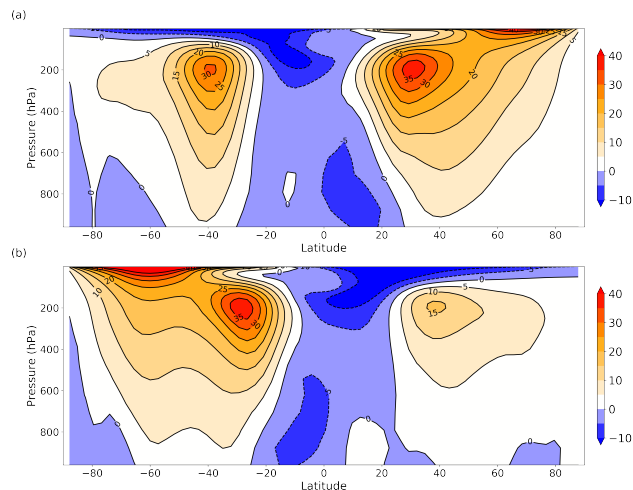
Figure 6. Time and zonal mean zonal wind velocities (m s^{-1}), for a) Winter (DJF) mean, and b) Summer (JJA) mean.

4.2 The Ocean

Annual mean SST (Fig. 7 a) shows maximum temperatures in the Indian and tropical Pacific and Atlantic Oceans reach 26°C. Compared with the Levitus climatology (Fig. 7 c) there is a cool bias of around 1°C throughout the tropics (Fig. 7 e). Regions immediately west of the major land masses (coincident with regions of coastal upwelling) show warm SST errors of 2-3°C
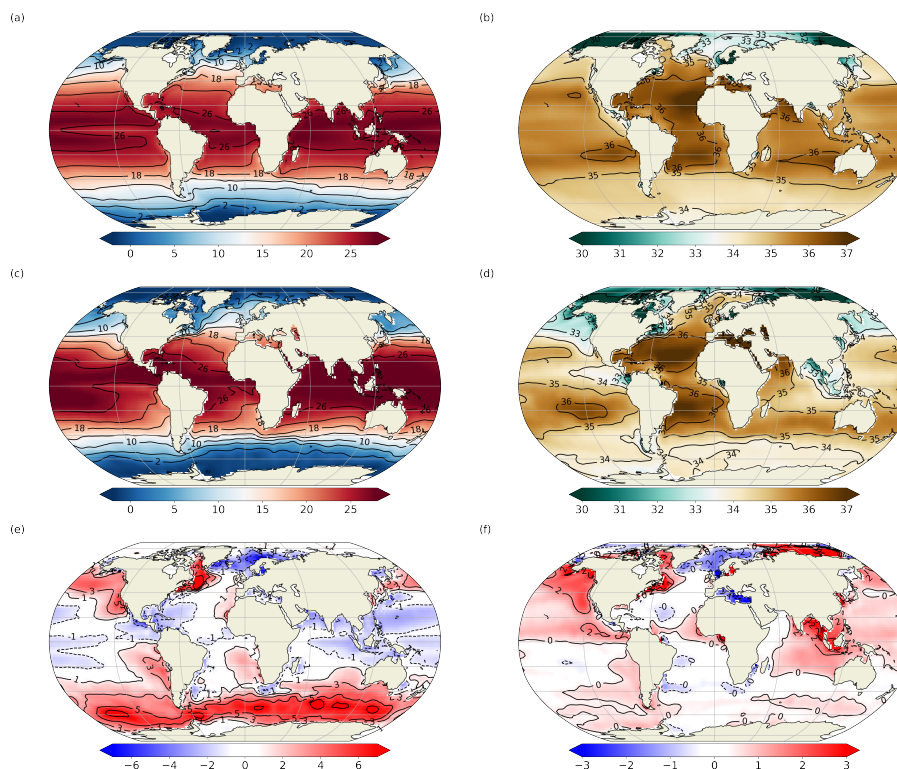
Figure 7. Time mean (years 2001-2025) of SST (left) and SSS (right) for FORTE 2.0 (top), EN3 (middle) and FORTE 2.0-EN3 anomalies.

magnitude, probably arising from a known issue in many coupled climate models related to the poor representation of marine stratocumulus cloud (Gordon et al., 2000). There is a substantial warm bias throughout the Southern Ocean and extending into the southern parts of the Pacific and Indian oceans, likely due to a combination of deficiencies in the physical representations of the ocean dynamics and cloud physics (Hyder et al., 2018). The Nordic Seas are several degrees cooler and up to 1.5 psu fresher than EN3, possibly due in part to the crude representation of sea ice, and in part due to the inadequate representation of ocean circulation in the Arctic and Nordic Seas in a 2° resolution ocean model. There is a positive salinity bias of around 3 psu further east in the Arctic, north of Siberia. Although large, the size of the salinity bias in the Arctic is not uncommon, even for models that do not require a polar island to prevent issues arising from the convergence of the grid at the north pole (Megann et al., 2010). Annual mean SSS is well represented throughout the southern hemisphere ocean, where errors are mainly confined to within +/- 0.5 psu (Fig. 7 f). Positive biases of order 1-1.5 psu occur in the Bay of Bengal and around the maritime continent and the northeast Pacific. The Labrador Sea and the region extending along the US coastline as far south as Cape Hatteras shows shows positive salinity biases between 0.5 and 2 psu, the latter coincident with a positive temperature bias that exceeds 5°C in a small region is indicative of the Gulf Stream separating too far north, bringing tropical waters too far north and west. Some of the model biases will arise from the relatively coarse horizontal and vertical resolution and missing
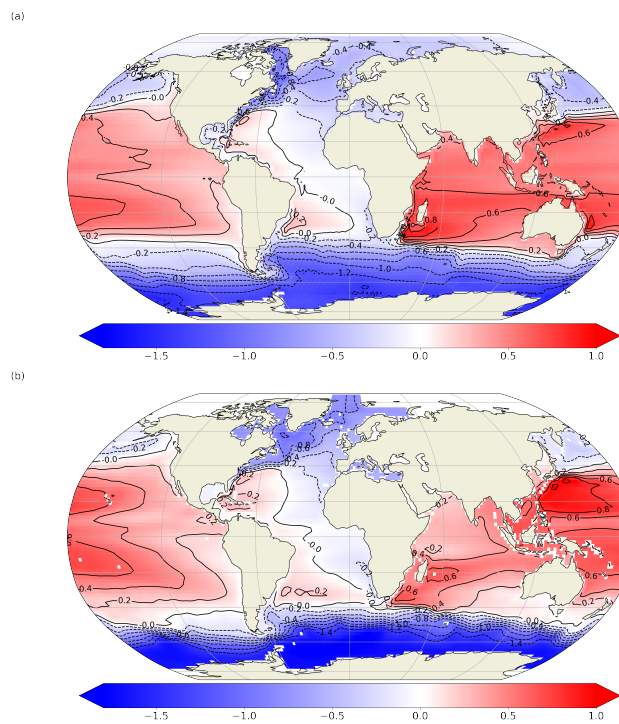
Figure 8. Time mean (years 2001-2025) of SSH for a) FORTE 2.0 and b) OCCA (2004-2006) climatology.
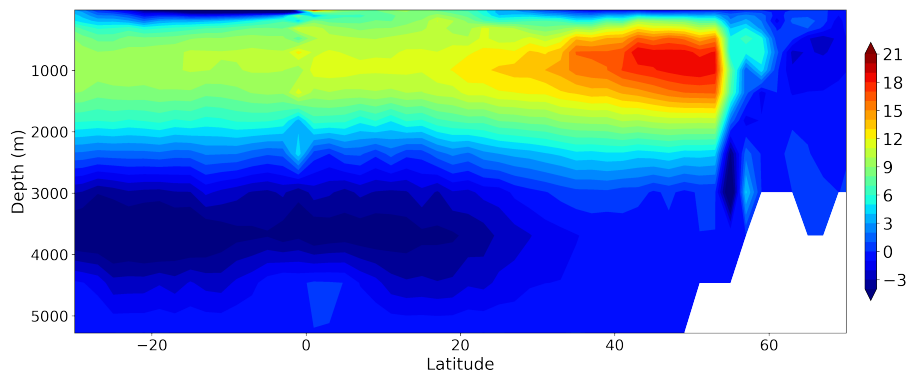
Figure 9. AMOC (Sv) as a function of latitude and depth, averaged over the control integration.
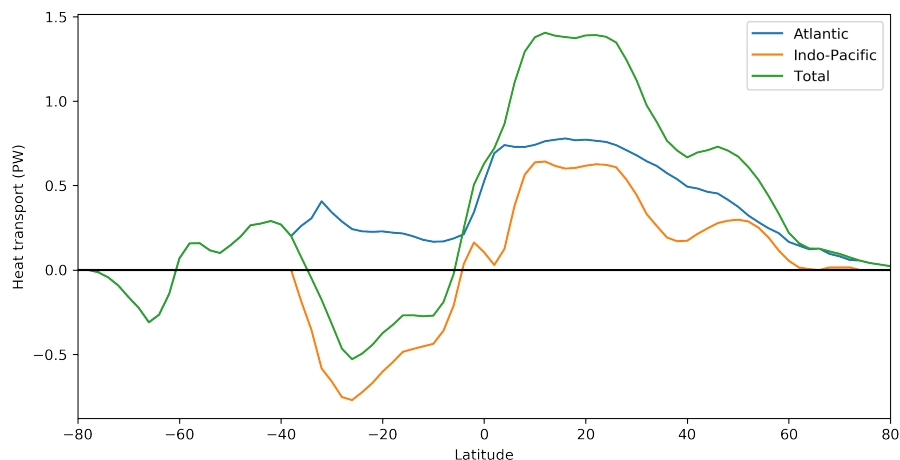
Figure 10. Meridional heat transport (PW) as a function of latitude for the Global ocean, Atlantic and Indo-Pacific, averaged over the control integration. A 3-grid point smoother has been applied.

physical processes. However, it is likely that a substantial reduction of biases would be achieved with the application of a rigorous calibration methodology such as History Matching (Williamson et al., 2014).

Sea surface height provides insight into the wind driven ocean circulation (Fig. 8). Gyre circulation in all the major ocean basins is highlighted by the contours, along with regions of intensified flow, such as the Gulf Stream, the Kuroshio, and along 5 the northern boundary of the ACC. However, the coarse resolution of the ocean model results in flows that are too broad and diffuse, weakening the SSH gradient across these intensified flows. The North Atlantic subpolar gyre appears constrained to the west of the basin. The slumping of the gradient across the ACC is evident, and corresponds to the weak ACC transport shown earlier (Fig. 3).

A latitude depth plot of the AMOC shows a maximum around 50°N and at 1000 m depth (Fig. 9). Deep convection occurs 10 in the high northern latitudes, and southward transport extends to around 3 km depth. The AMOC transport through 30°S is 10 Sv, and is stronger (~14 Sv) at 30°N. There is a strong Antarctic Bottom Water Cell (~6 Sv) centered at about 3500 m depth, which weakens to about 2 Sv at 30°N. Sinking at the high northern latitudes occurs abruptly in a narrow latitude band, not uncharacteristic of coarse resolution ocean models where flow into the Nordic Seas is poorly represented. There is evidence of two grid point noise at the Equator, which has been identified previously in Bryan-Cox models (Weaver and Sarachik, 1990).

15 Ocean meridional heat transport (OHT) in FORTE 2.0 is around 60% that expected based on observational estimates, but consistent with the weaker than observed volume transport (Fig. 10). Atlantic OHT at 26°N is 0.74 PW, whilst observationally derived estimates suggest the current value is closer to 1.3 PW (Johns et al., 2011). Globally, the OHT reaches 1.4 PW, instead of the 2.1 ± 0.3 PW computed by Trenberth and Caron (2001). Over the Southern Ocean (35-65°S) OHT is northward, a
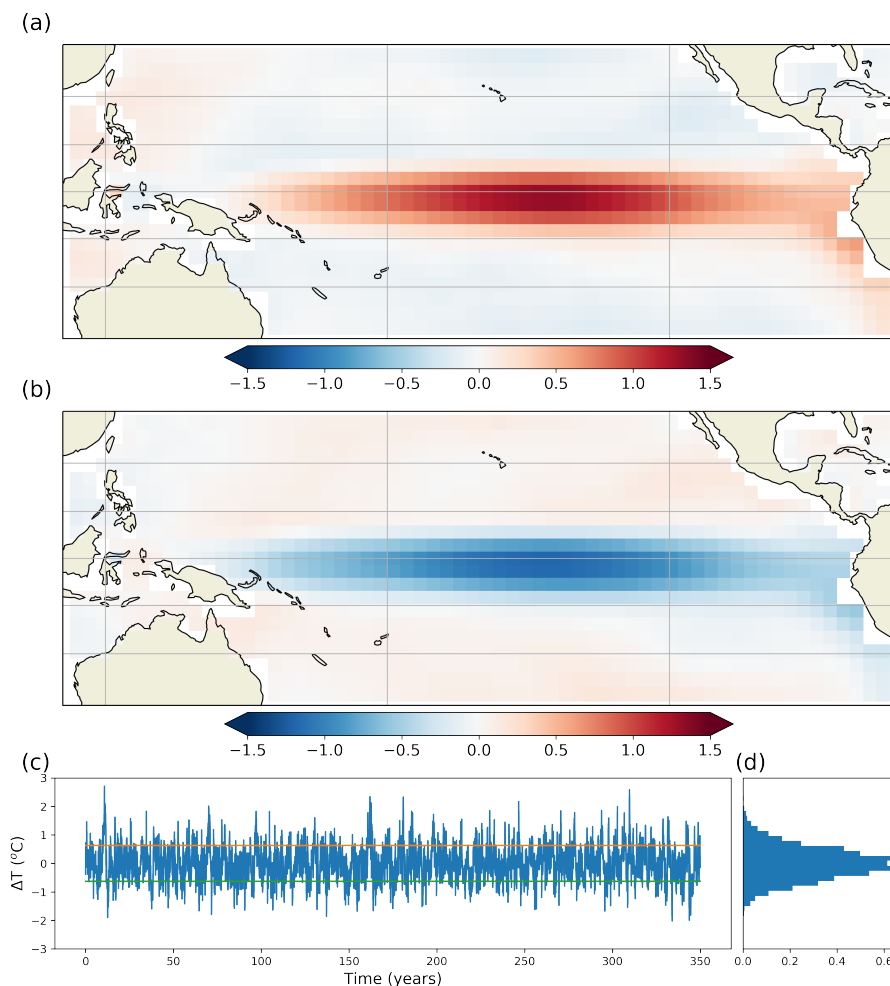
Figure 11. Composite anomaly of a) El Niño events, and b) La Niña events. ENSO events are defined as those which exceed 1 standard deviation anomaly within the Niño 3.4 region. SST anomaly time series for years 1601-1950 (c)), and histogram of SST anomaly distribution relative to the mean (d)) for the region Niño 3.4.

characteristic seen previously in MOM-based ocean models (de Freitas Assad et al., 2009). This may be related to the strong warm SST bias present over region 40-60°S (Fig. 7) and its consequent effect on surface heat fluxes.

5 Modes of variability

A primary aim for any climate model is to adequately reproduce observed modes of climate variability sufficiently well that the model can be used to study the observed phenomena in a variety of contexts. In this section we present analysis of some
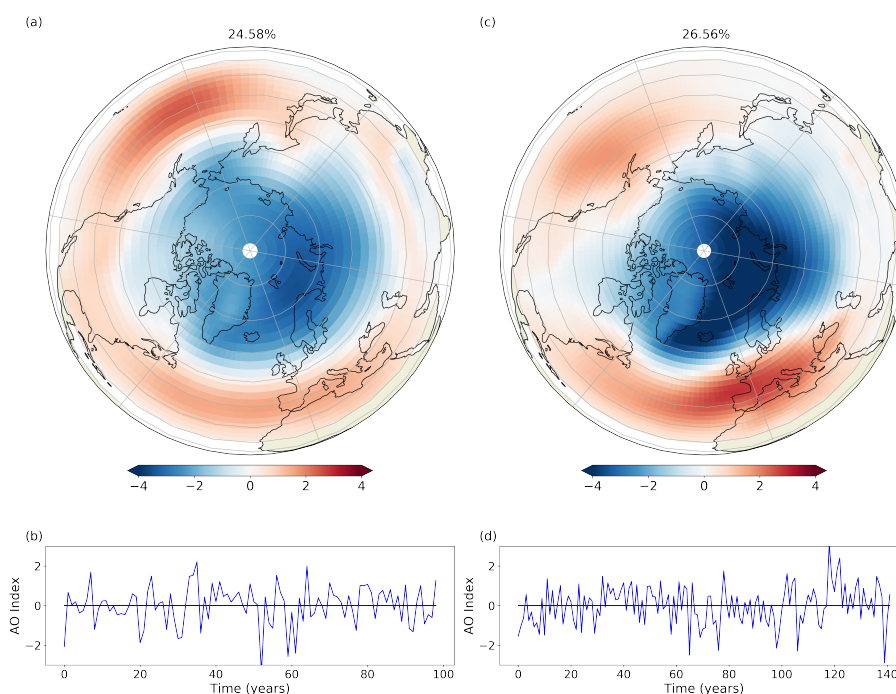
Figure 12. The AO as represented by the first EOF and PC computed using deseasoned and latitude weighted sea level pressure for FORTE 2.0 (a,b), and 20th Century Reanalysis (c, d)
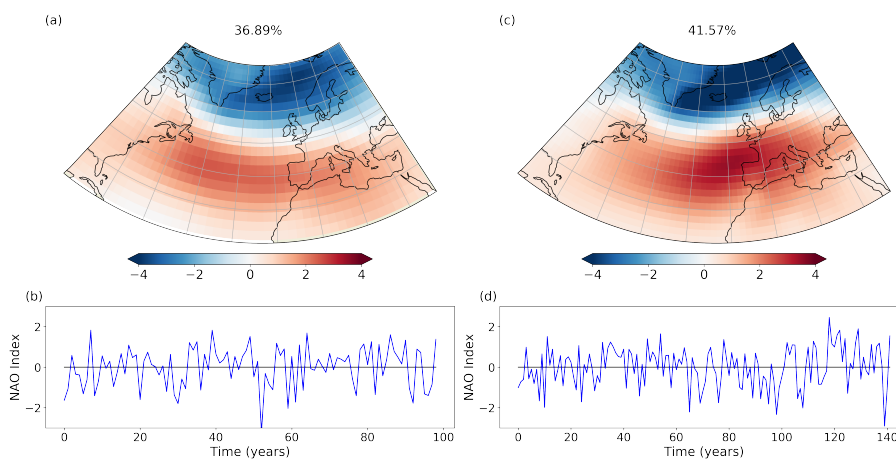
Figure 13. The NAO as represented by the first EOF and PC computed using deseasoned and latitude weighted sea level pressure for FORTE 2.0 (a, b), and 20th Century Reanalysis (c, d)
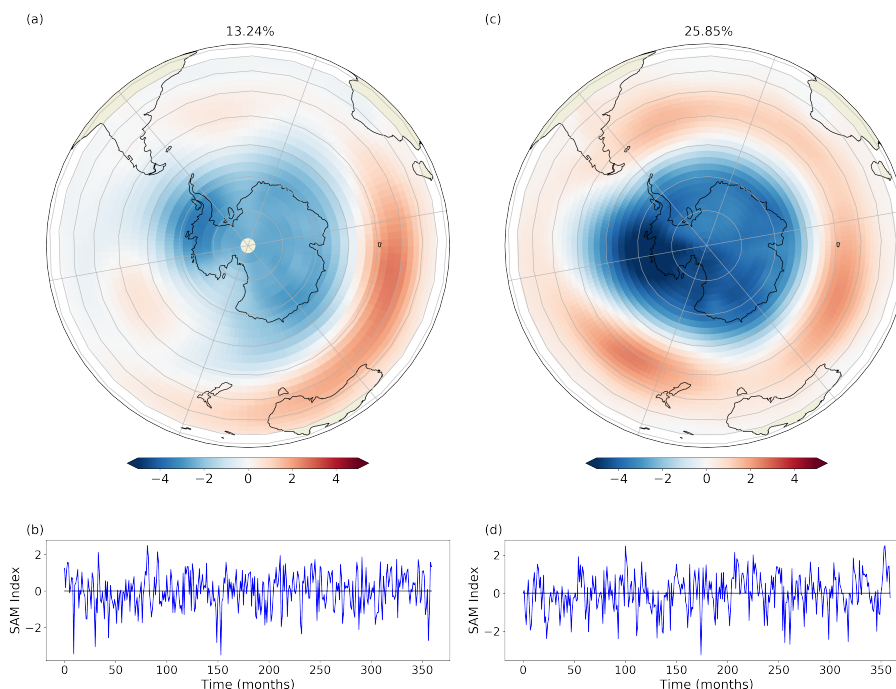
Figure 14. The SAM as represented by the first EOF and PC computed using deseasoned and latitude weighted sea level pressure for FORTE 2.0 (a, b), and 20th Century Reanalysis (c, d)

of the most important modes using monthly mean ocean output for the years 1600-1950 of the control simulation and daily surface pressure output during years 1600-1699 of the control integration.

Composites of the SST anomaly during El Niño and La Niña years show the spatial pattern of the anomalies throughout the tropics (Fig. 11 a, b). Both phases of ENSO are weaker than observed, in particular nearer the eastern boundary. The composite temperature anomaly reaches a maximum of 1°C for the region 160°W-100°W, 5°S-5°N, whilst the characteristic region of observed strong SST anomalies near to the coast of central and southern America only reaches 0.7°C and is not strongly connected to the warm anomaly in the central Pacific. This is probably related to the fact that the South Pacific Convergence Zone is too zonal and extends all the way across the Pacific, which is a common feature in coupled climate models (Niznik et al., 2015). The time series of temperature anomalies in the Niño 3.4 region shows a number of strong temperature anomaly events, although the magnitude is in general too small (Fig. 11 c, d). The tails of the histogram extend to around ±2°(Fig 11 d)), whilst a similar plot of observations between 1950 and 1997 suggests the extremes should be closer to ±2.5° (Fig. 2 from Trenberth (1997)).

We also examine the main extratropical modes of variability predicted by FORTE 2.0 in the northern hemisphere. We compare empirical orthogonal function (EOF) analysis of the deseasoned and latitude weighted sea level pressure fields from FORTE 2.0 and, for comparison, the 20th Century Reanalysis (Compo et al., 2011). FORTE 2.0 produces an annular mode

structure as the main mode of variability, corresponding to the Arctic Oscillation in observed data. In agreement with observations (e.g. Thompson and Wallace, 2000; Ambaum et al., 2001), the model reproduces the two mid latitude centres of action over the North Pacific and North Atlantic, with the Pacific centre stronger and the Atlantic centre slightly weaker than those seen in the 20th Century Reanalysis and the locations of their maxima displaced westward towards the western half of each

5 ocean basin (Fig. 12). The strength of the Arctic pole in FORTE is also weaker than observations. Comparison of the corresponding principal component time-series (Fig. 12) suggests the presence of some higher frequency variability in observations that is not captured by FORTE 2.0. The North Atlantic Oscillation (NAO) is closely related to the AO and is one of the principal modes of atmospheric variability in the North Atlantic sector (Hurrell, 1995). The first EOF and its accompanying principal component are presented in Fig. 13. In the North Atlantic there is a good approximation to the NAO pattern, but in FORTE

10 2.0 the centre of the southern lobe is displaced westward and the northern lobe extends further south over mainland Europe compared with the observed pattern. Again, the principal component suggests more high-frequency variability in observations than FORTE 2.0.

Similar to the northern hemisphere, the Southern Annular Mode, or Antarctic Oscillation represents the principal mode of climate variability in the southern hemisphere. FORTE performs less well in the southern hemisphere (Fig. 14), with the

15 annular structure significantly weaker over the Pacific and Atlantic sectors. The variance explained by the first EOF is also greatly reduced in FORTE, approximately half that seen in the 20th Century Reanalysis, and is likely to be linked with the anomalously warm Southern Ocean SST.

6 Summary

We present an assessment of a 2000 year control simulation of the FORTE 2.0 coupled climate model. The model integrates

20 from rest and is sufficiently fast to enable studies of multi-centennial climate variability. The model is economic to run, and can be adapted and configured to study a wide range of climate questions.

The simulation presented here is not optimally tuned for any specific purpose, but our assessment indicates that FORTE 2.0 is able to simulate a satisfactory climate state and climate variability. Biases that develop in the mean state are comparable to those found in other coupled climate models (Flato et al., 2013) and particularly those of similar complexity and resolution.

25 A small imbalance in the fresh water budget (see Fig. 2) would need to be addressed for studies extending over timescales much longer than several millennia. Modes of climate variability in the northern hemisphere are represented well, though there are shortcomings in the southern hemisphere variability that are likely related to a strong SST bias over the Southern Ocean. Identifying the cause(s) of such biases is often a complex process in itself (Hyder et al., 2018), and beyond the scope of this current work. A further step would be to rigorously calibrate the model to improve the simulated climate and to better

30 understand the limitations and behaviour of the modelled climate system.

7 Code availability

The code, compilation instructions and example run scripts, together with all necessary ancillary files are accessible at: http://doi.org/10.5281/zenodo.3632569. The configuration committed to the Zenodo archive is the one used to produce the simulation presented in this paper. Processing of the IGCM4 output requires the program BGFLUX, a copy of which is accessible from the FORTE2.0 GitHub repository linked to the Zenodo archive. A comprehensive user guide/manual for FORTE 2.0 does not currently exist. A folder titled Documentation has been added to the FORTE2.0 GitHub repository, and this contains relevant references and copies of technical documents from the original FORTE and component models.

8 Data availability

The code and data required to reproduce the figures presented in this paper are provided in a supplementary file.

Author contributions. ATB, MJ and BS developed the coupled model configuration from versions used in earlier studies. The original coupling of FORTE was performed by BS and RSS. All authors were involved in finalising the configuration presented here. MJ undertook all model simulations. ATB wrote the paper, analysed the output and prepared all tables and figures. All authors edited the paper text.

Competing interests. The authors declare that they have no competing interests.

Acknowledgements. We acknowledge the support of resources provided by the High Performance Computing Cluster supported by the Research and Specialist Computing Support service at the University of East Anglia. We also acknowledge the support and contributions from colleagues on earlier versions of the code and simulations, most notably M. Brand, C. Wallace, and M. Stringer. We gratefully acknowledge the developers of the software packages PVM and OASIS2.3, both of which are instrumental in the coupling for FORTE 2.0. ATB and BS received support from ACSIS (NE/N018044/1); BS was also supported by SMURPHS (NE/N005686/2). MJ was partially funded by SMURPHS (NE/N006348/1).

References

Adler, R. F., R.F., Huffman, G., Chang, A., Ferraro, R., Xie, P. P., Janowiak, J., Rudolf, B., Schneider, U., Curtis, S., Bolvin, D., Gruber, A., Susskind, J., Arkin, P., , and Nelkin, E.: The Version-2 Global Precipitation Climatology Project (GPCP) Monthly Precipitation Analysis (1979–Present), Journal of Hydrometeorology, 4, 1147–1167, 2003.

Ambaum, M. H. P., Hoskins, B. J., and Stephenson, D. B.: Arctic Oscillation or North Atlantic Oscillation?, Journal of Climate, 14, 3495–3507, 2001.

Arakawa, A.: Computational design for long-term numerical integrations of the equations of atmospheric motion, Journal of Computational Physics, 1, 119–143, 1966.

Atkinson, C. P., Wells, N. C., Blaker, A. T., Sinha, B., and Ivchenko, V. O.: Rapid ocean wave teleconnections linking Antarctic salinity anomalies to the equatorial ocean-atmosphere system, Geophysical Research Letters, 36, doi:10.1029/2008GL036976, 2009.

Betts, A. K. and Miller, M. J.: The Betts-Miller scheme, in: The representation of cumulus convection in numerical models of the atmosphere, Eds. K.A. Emanuel and D.J. Raymond, 1993.

Blaker, A. T., Sinha, B., Ivchenko, V. O., Wells, N. C., and Zalesny, V. B.: Identifying the roles of the ocean and atmosphere in creating a rapid equatorial response to a Southern Ocean anomaly, Geophysical Research Letters, 33, L06720, doi:10.1029/2005GL025474, 2006.

Buchan, J., Hirschi, J. J.-M., Blaker, A. T., and Sinha, B.: North Atlantic SST anomalies and the cold North European weather events of winter 2009/10 and December 2010, Monthly Weather Review, 142, 922–932, doi:10.1175/MWR-D-13-00104.1, 2014.

Compo, G. P., S.Whitaker, J., Sardeshmukh, P. D., Matsui, N., Allan, R. J., Yin, X., B. E. Gleason, J., Vose, R. S., Rutledge, G., Bessemoulin, P., Brönnimann, S., Brunet, M., Crouthamel, R. I., Grant, A. N., Groisman, P. Y., Jones, P. D., Kruk, M. C., Kruger, A. C., Marshall, G. J., Maugeri, M., Mok, H. Y., Nordli, Ø., Ross, T. F., Trigo, R. M., Wang, X. L., Woodruff, S. D., and Worley, S. J.: The Twentieth Century Reanalysis Project, Quarterly Journal of the Royal Meteorological Society, 137, 1–28, 2011.

Cunningham, S. A., Alderson, S., King, B., and Brandon, M.: Transport and variability of the Antarctic Circumpolar Current in Drake Passage, Journal of Geophysical Research, 108, 8084, doi:10.1029/2001JC001147, 2003.

Danabasoglu, G. and McWilliams, J. C.: Sensitivity of the global ocean circulation to parameterizations of mesoscale tracer transports, Journal of Climate, 8, 2967–2987, 1995.

de Freitas Assad, L. P., Torres, A. R., Arruda, W. Z., da Silveira Mascarenhas, A., and Landau, L.: Volume and heat transports in the world oceans from an ocean general circulation model, Brazilian Journal of Geophysics, 27, 181–194, doi:10.1590/S0102-261X2009000200003, 2009.

Donohue, K. A., Tracey, K. L., Watts, D. R., Chidichimo, M. P., and Chereskin, T. K.: Mean Antarctic Circumpolar Current transport measured in Drake Passage, Geophysical Research Letters, 43, 11 760–11 767, doi:10.1002/2016GL070319, 2016.

ETOPO5: Global 5' x 5' depth and elevation. Technical report, National Geophysical Data Centre, NOAA, US Department of Commerce, Boulder, USA, 1988.

Eyring, V., Bony, S., Meehl, G. A., Senior, C. A., Stevens, B., Stouffer, R. J., and Taylor, K. E.: Overview of the Coupled Model Intercomparison Project Phase 6 (CMIP6) experimental design and organization, Geoscientific Model Development, 9, 1937–1958, doi:10.5194/gmd-9-1937-2016, 2016.

Flato, G., Marotzke, J., Abiodun, B., Braconnot, P., Chou, S. C., Collins, W., Cox, P., Driouech, F., Emori, S., Eyring, V., Forest, C., Gleckler, P., Guilyardi, E., Jakob, C., Kattsov, V., Reason, C., and Rummukainen, M.: Evaluation of climate models, pp. 741–882, T. F. Stocker, D.

Qin, G.-K. Plattner, M. Tignor, S. K. Allen, J. Doschung, A. Nauels, Y. Xia, V. Bex, and P. M. Midgley, Eds, Cambridge University Press, Cambridge, UK, doi:10.1017/CBO9781107415324.020, 2013.

Forster, P. M., Blackburn, M., and Glover, R.: An examination of climate sensitivity for idealised climate change experiments in an intermediate general circulation model, Climate Dynamics, 16, 833–849, 2000.

5 Gargett, A. E.: Vertical eddy diffusivity in the ocean interior, Journal of Marine Research, 42, 359–393, doi:10.1357/002224084788502756, 1984.

Geist, A., Beguelin, A., Dongarra, J., Jiang, W., Manchek, R., and Sunderam, V.: PVM: parallel virtual machine, MIT Press, Cambridge, Massachusetts, 1994.

Gent, P. R. and McWilliams, J. C.: Isopycnal mixing in ocean circulation models, Journal of Physical Oceanography, 20, 150–155, 1990.

10 Gordon, C., Cooper, C., Senior, C., Banks, H., Gregory, J., Johns, T., Mitchell, J., and Wood, R.: The simulation of SST, sea ice extents and ocean heat transports in a version of the Hadley Centre coupled model without flux adjustments, Climate Dynamics, 16, 147–168, 2000.

Griffies, S. M.: The Gent-McWilliams skew flux, Journal of Physical Oceanography, 28, 831–841, 1998.

Griffies, S. M., Gananadesikan, A., Pacanowski, R. C., Larichev, V., Dukowicz, J., and Smith, R.: Isoneutral diffusion in a z-coordinate ocean model, Journal of Physical Oceanography, 28, 805–830, 1998.

15 Grist, J. P., Josey, S. A., Sinha, B., and Blaker, A. T.: Response of the Denmark Strait overflow to Nordic Seas heat loss, Journal of Geophysical Research, 113, 10.1029/2007JC004 625, 2008.

Haarsma, R. J., Selten, F. M., Opsteegh, J. D., Lenderink, G., and Liu, Q.: A coupled Atmosphere Ocean Sea-ice model for climate predictability studies, Technical Report, KNMI, The Netherlands, 1996.

Haarsma, R. J., Roberts, M. J., Vidale, P. L., Senior, C. A., Bellucci, A., Bao, Q., Chang, P., Corti, S., Fučkar, N. S., Guemas, V., von
20 Hardenberg, J., Hazeleger, W., Kodama, C., Koenigk, T., Leung, L. R., Lu, J., Luo, J.-J., Mao, J., Mizielinski, M. S., Mizuta, R., Nobre, P., Satoh, M., Scoccimarro, E., Semmler, T., Small, J., and von Storch, J.-S.: High Resolution Model Intercomparison Project (HighResMIP v1.0) for CMIP6, Geoscientific Model Developments, 9, 4185–4208, doi:10.5194/gmd-9-4185-2016, 2016.

Heuzé, C., Heywood, K., Stevens, D., and Ridley, J.: Changes in Global Ocean Bottom Properties and Volume Transports in CMIP5 Models under Climate Change Scenarios, Journal of Climate, 28, 2917–2944, doi:10.1175/JCLI-D-14-00381.1, 2015.

25 Hunt, F. K., Hirschi, J. J.-M., Sinha, B., Oliver, K., and Wells, N.: Combining point correlation maps with self-organising maps to compare observed and simulated atmospheric teleconnection patterns, Tellus A, 65, doi:10.3402/tellusa.v65i0.20822, 2013.

Hurrell, J. W.: Decadal trends in the North Atlantic Oscillation regional temperatures and precipitation, Science, 269, 676–679, 1995.

Hyder, P., Edwards, J. M., Allan, R. P., Hewitt, H. T., Bracegirdle, T. J., Gregory, J. M., Wood, R. A., Meijers, A. J. S., Mulcahy, J., Field, P., Furtado, K., Bodas-Salcedo, A., Williams, K. D., Copsey, D., Josey, S. A., Liu, C., Roberts, C. D., Sanchez, C., Ridley, J., Thorpe, L.,
30 Hardiman, S. C., Mayer, M., Berry, D. I., and Belcher, S. E.: Critical Southern Ocean climate model biases traced to atmospheric model cloud errors, Nature Communications, 9, doi:10.1038/s41467-018-05634-2, 2018.

Johns, T. C., Durman, C. F., Banks, H. T., Roberts, M. J., McLaren, A. J., Ridley, J. K., Senior, C. A., Williams, K. D., Jones, A., Rickard, G. J., Cusack, S., Ingram, W. J., Crucifix, M., Sexton, D. M. H., Joshi, M. M., Dong, B. W., Spencer, H., Hill, R. S. R., Gregory, J. M., Keen, A. B., Pardaens, A. K., Lowe, J. A., Bodas-Salcedo, A., and Stark, S.: The New Hadley Centre Climate Model (HadGEM1):
35 Evaluation of Coupled Simulations, Journal of Climate, 19, 1327–1353, 2006.

Johns, W. E., Baringer, M. O., Beal, L. M., Cunningham, S. A., Kanzow, T., Bryden, H. L., Hirschi, J. J.-M., Marotzke, J., Meinen, C., Shaw, B., and Curry, R.: Continuous, array-based estimates of Atlantic Ocean heat transport at 26.5N, Journal of Climate, 24, 2429–2449, doi:10.1175/2010JCLI3997.1, 2011.

Joshi, M., Stringer, M., van der Wiel, K., O'Callaghan, A., and Fueglistaler, S.: IGCM4: a fast, parallel and flexible intermediate climate model, Geoscientific Model Development, 8, 1157–1167, 2015.

Killworth, P. D., Stainforth, D., Webb, D. J., and Paterson, S. M.: The development of a free-surface Bryan-Cox-Semtner ocean model, Journal of Physical Oceanography, 21, 1333–1348, 1991.

5 Levitus, S. and Boyer, T. P.: World Ocean Atlas 1998, Volume 4, Temperature., NOAA Atlas, NESDIS 2, 99pp, 1998.

Levitus, S., Burgett, R., and Boyer, T. P.: World Ocean Atlas 1998, Volume 3, Salinity., NOAA Atlas, NESDIS 3, 99pp, 1998.

Marsh, R., Hazeleger, W., Yool, A., and Rohling, E. J.: Stability of the thermohaline circulation under millennial CO_2 forcing and two alternative controls on Atlantic salinity, Geophysical Research Letters, 34, doi:10.1029/2006GL027815, 2007.

McCarthy, G., Frajka-Williams, E., Johns, W. E., Baringer, M. O., Meinen, C. S., Bryden, H. L., Rayner, D., Duchez, A., Roberts, C., and

10 Cunningham, S. A.: Observed interannual variability of the Atlantic meridional overturning circulation at 26.5N, Geophysical Research Letters, 39, doi:10.1029/2012GL052933, 2012.

Meehl, G. A., Covey, C., Delworth, T., Latif, M., McAvaney, B., Mitchell, J., Stouffer, R., and Taylor, K.: The WCRP CMIP3 Multimodel Dataset: A New Era in Climate Change Research, Bulletin of the American Meteorlogical Society, 88, 1383–1394, 2007.

Megann, A. P., New, A. L., Blaker, A. T., and Sinha, B.: The CHIME coupled climate model, Journal of Climate, xx, 2010.

15 Montoya, M., Griesel, A., Levermann, A., Mignot, J., Hofmann, M., Ganopolski, A., and Rahmstorf, S.: The earth system model of intermediate complexity CLIMBER-3-alpha. Part I: description and performance for present-day conditions, Climate Dynamics, 25, 237–263, doi:10.1007/s00382-005-0044-1, 2005.

Niznik, M. J., Lintner, B., Matthews, A., and Widlansky, M.: The Role of Tropical–Extratropical Interaction and Synoptic Variability in Maintaining the South Pacific Convergence Zone in CMIP5 Models, Journal of Climate, 28, 3353–3374, doi:10.1175/JCLI-D-14-00527.1,

20 2015.

Pacanowski, R. C., Dixon, K., and Rosati, A.: The GFDL modular ocean model users guide: version 1.0, GFDL Group Technical Report No. 2, Tech. rep., NOAA/Geophysical Fluid Dynamics Laboratory, Princeton University, Princeton, NJ, variously paged, 1990.

Roberts, M. J., Baker, A., Blockley, E. W., Calvert, D., Coward, A., Hewitt, H. T., Jackson, L. C., Kuhlbrodt, T., Mathiot, P., Roberts, C. D., Schiemann, R., Seddon, J., Vannière, B., and Vidale, P. L.: Description of the resolution hierarchy of the global coupled HadGEM3-GC3.1

25 model as used in CMIP6 HighResMIP experiments, Geoscientific Model Developments, 12, 4999–5028, doi:10.5194/gmd-12-4999-2019, 2019.

Russell, J. L., Stouffer, R. J., and Dixon, K. W.: Intercomparison of the Southern Ocean circulation in IPCC coupled model control simulations, Journal of Climate, 19, 4560–4575, doi:10.1175/JCLI3869.1, 2006.

Sellar, A. A., Jones, C. G., Mulcahy, J. P., Tang, Y., Yool, A., Wiltshire, A., O'Connor, F. M., Stringer, M., Hill, R., Palmieri, J., Woodward,

30 S., de Mora, L., Kuhlbrodt, T., Rumbold, S. T., Kelley, D. I., Johnson, R. E. C. E., Walton, J., Abraham, N. L., Andrews, M. B., Andrews, T., Archibald, A. T., Berthou, S., Burke, E., Blockley, E., Dalvi, K. C. M., Edwards, J., Folberth, G. A., Gedney, N., Griffiths, P. T., Harper, A. B., Hendry, M. A., Hewitt, A. J., Johnson, B., Jones, A., Jones, C. D., Keeble, J., Liddicoat, S., Morgenstern, O., Parker, R. J., Predoi, V., Robertson, E., Siahaan, A., Smith, R. S., Swaminathan, R., Zeng, M. T. W. G., and Zerroukat, M.: UKESM1: Description and Evaluation of the U.K. Earth System Model, Journal of Advances in Modelling Earth Systems, 11, doi:10.1029/2019MS001739, 2019.

35 Shaffrey, L. C., Stevens, I., Norton, W. A., Roberts, M. J., Vidale, P. L., Harle, J. D., Jrrar, A., Stevens, D. P., Woodage, M. J., Demory, M. E., Donners, J., Clark, D. B., Clayton, A., Cole, J. W., Wilson, S. S., Connolley, W. M., Davies, T. M., Iwi, A. M., Johns, T. C., King, J. C., New, A. L., Slingo, J. M., Slingo, A., Steenman-Clark, L., and Martin, G. M.: UK-HiGEM: The New UK High Resolution Global Environment Model. Model description and basic evaluation, Journal of Climate, doi:10.1175/2008JCLI2508.1, 2009.

Sinha, B. and Smith, R.: Development of a fast Coupled General Circulation Model (FORTE) for climate studies, implemented using the OASIS coupler, Tech. rep., Southampton Oceanography Centre, Internal Document, No. 81, 67pp., 2002.

Sinha, B., Blaker, A. T., Hirschi, J. J.-M., Bonham, S., Brand, M., Josey, S. A., Smith, R. S., and Marotzke, J.: Mountain ranges favour vigorous Atlantic meridional overturning, Geophysical Research Letters, 39, doi:10.1029/2011GL050485, 2012.

5 Smith, R., Dubois, C., and Marotzke, J.: Ocean circulation and climate in an idealised Pangean OAGCM, Geophysical Research Letters, 31, doi:10.1029/2004GL020643, 2004.

Smith, R., Dubois, C., and Marotzke, J.: Global Climate and Ocean Circulation on an Aquaplanet Ocean-Atmosphere General Circulation Model, Journal of Climate, 19, 4719–4737, 2006.

Smith, R., Gregory, J. M., and Osprey, A.: A description of the FAMOUS (version XDBUA) climate model and control run, Geoscientific

10 Model Developments, 1, 53–68, 2008.

Taylor, K., Stouffer, R., and Meehl, G.: An Overview of CMIP5 and the experiment design, Bulletin of the American Meteorological Society, 93, 485–498, doi:10.1175/BAMS-D-11-00094.1, 2012.

Terray, L., Valcke, S., and Piacentini, A.: The OASIS Coupler User Guide Version 2.3, Tech. Rep. TR/CMGC/99-37, Tech. rep., CERFACS, Toulouse, France,, 1999.

15 Thompson, D. W. J. and Wallace, J. M.: Annular modes in the extratropical circulation. Part I: Month-to-month variability, Journal of Climate, 13, 1000–1016, 2000.

Trenberth, K. E.: The definition of El Nino, Bulletin of the American Meteorological Society, 78, 2771–2777, 1997.

Trenberth, K. E. and Caron, J. M.: Estimates of meridional atmosphere and ocean heat transports, Journal of Climate, 14, 3433–3443, 2001.

Weaver, A. J.: The UVic earth system climate model and the thermohaline circulation in past, present and future climates, IUGG 2003

20 General Assembly of the International Union of Geodesy and Geophysics No23, Sapporo, Geophysical monograph ISSN 0065-8448 CODEN GPMGAD, 150 (416p.), 279–296, 2004.

Weaver, A. J. and Sarachik, E. S.: On the importance of vertical resolution in certain ocean general circulation models, Journal of Physical Oceanography, 20, 600–609, 1990.

Webb, D. J.: An ocean model code for array processor computers, Computers and Geosciences, 22, 569–578, 1996.

25 Webb, D. J., de Cuevas, B. A., and Richmond, C. S.: Improved Advection Schemes for Ocean Models, J. Atmos. Oceanic Technology, 15, 1171–1187, 1998.

Williamson, D., Blaker, A. T., Hampton, C., and Salter, J.: Identifying and removing structural biases in climate models with history matching, Climate Dynamics, 45, 1299–1324, 2014.

Wilson, C., Sinha, B., and Williams, R. G.: The effect of ocean dynamics and orography on atmospheric storm tracks, Journal of Climate,

30 doi:10.1175/2009JCLI2651.1, 2009.

Wu, J.: Wind-Stress Coefficients over Sea Surface near Neutral Conditions - A Revisit, Journal of Physical Oceanography, 10, 727–740, 1980.